Heterogeneous & Homogeneous & Bio- & Nano-

CHEMCATCHEM

CATALYSIS

Accepted Article

Title: Changing the Product Selectivity for Electrocatalysis of CO2 Reduction Reaction on Plated Cu Electrodes

Authors: Hong Li, Xianxian Qin, Tian-Wen Jiang, Xian-Yin Ma, Kun Jiang, and Wen-Bin Cai

To be cited as: *ChemCatChem* 10.1002/cctc.201901748

Link to VoR: http://dx.doi.org/10.1002/cctc.201901748

A Journal of

ChemPubSoc Europe

WILEY-VCH

www.chemcatchem.org

10.1002/cctc.201901748

Changing the Product Selectivity for Electrocatalysis of CO_2 Reduction Reaction on Plated Cu Electrodes

Hong Li, [a] Xianxian Qin, [a] Tianwen Jiang, [a] Xian-Yin Ma, [a] Prof. Dr. Kun Jiang,*[b] Prof. Dr. Wen-Bin Cai*[a]

[a] Shanghai Key Laboratory of Molecular Catalysis and Innovative Materials, Collaborative Innovation Center of Chemistry for Energy Materials, Department of Chemistry, Fudan University, Shanghai 200438, China.
Email: wbcai@fudan.edu.cn.

[b] Institute of Fuel Cells, School of Mechanical Engineering, Shanghai Jiao Tong University, Shanghai 200240, China.
Email: kunjiang@sjtu.edu.cn.

Invited contribution to the Special Issue:
Electrocatalysis: From Batteries to Clean Energy Conversion

Abstract

Electrochemical reduction of carbon dioxide (CO_2RR) on various types of Cu electrodes to useful chemicals and fuels has attracted much attention. Herein, we comparatively investigate the distributions of CO_2RR products over electroplated Cu, chemically plated boron-doped Cu (Cu-B) and electroplated phosphorus-doped Cu (Cu-P) electrodes. A global Faradaic efficiency of more than 50% can be reached for the C2+ (ethylene, ethanol and n-propanol) products on both plated Cu-B and Cu-P electrodes at ~ -1.15 V vs. RHE in 0.1 M $KHCO_3$ electrolyte. Moreover, *in situ* surface enhanced infrared spectroscopy results together with quantitative analysis of the CO_2RR products reveal a more facile conversion/depletion of the *CO intermediate after B- and P-doping, for which Cu-B promotes the C2+ products while Cu-P enhances both C2+ generation and CH_4 evolution at faster *CO consumption. The present work suggests the vital role of *CO in the step of C-C bonding formation and highlights that the metalloid doping may alter the reactivity and selectivity of the intermediate.

Introduction

Electrochemical CO_2 reduction to value-added chemicals using renewable energies has attracted significant attention as a potential solution to reduce anthropogenic carbon emissions as well as to fulfill clean electricity storage.[1] Among CO_2 reduction products, C2+ hydrocarbons and oxygenates like ethylene (C_2H_4), ethanol (C_2H_5OH) and n-propanol are highly desirable owing to their impressive energy densities as compared to C1 compounds.[2] Copper (Cu) is the only metal capable of reducing CO_2 to multi-carbon products at relatively high yields, though still challenged by the H_2 evolution side reaction and the simultaneous generation of other C1 products like CO and CH_4 in aqueous electrolytes.[3]

So far, different strategies have been proposed to optimize the structure and composition of Cu-based catalysts toward selective multi-carbons products generation.[4] Earlier single crystalline studies suggest that Cu(100) is more selective for C_2H_4 generation vs. CH_4 evolution as compared to Cu(111).[5] For poly-crystalline Cu electrodes, the control over morphology,[6] nanoparticle size,[7] surface roughness[8] grain boundary density[9] has been demonstrated to tune up the C2+ selectivity as well. As for the component optimization, the alloying of Cu with Pd,[10]Ag[9b, 11] or Zn[12] has been proposed to improve the selectivity toward ethylene and ethanol products. Recently, the incorporation of a metalloid component to modify the electronic structure and thus tuning the binding strength of metal surfaces has attracted considerable interest. Our earlier study on boron-doped Pd catalyst reveals the enhanced formate production over a wide potential window as compared to un-doped Pd, resulting from a downshifted d-band center of surface Pd atoms with B doping.[13] Along this line, metalloid doped Cu catalysts, such as Cu-S,[14] Cu-B[15] and Cu-N catalysts[16] have been explored as well for the CO_2RR. Varying the metalloid component may lead to different product distributions. Specifically, that the Cu-S catalyst promotes the C1 products while the other two favor the C2+ products. As the C2+ products promoters, the previous Cu-B and Cu-N catalysts were prepared via wet-chemical synthesis,[15a] high temperature calcination,[15b] and hydrothermal synthesis.[16] The catalysts thus obtained are hardly applicable for in situ spectroelectrochemical measurements.

In addition to the above efforts, a better understanding of the Cu electrode/electrolyte interface is highly demanded for developing Cu-based catalysts as the electrochemical CO_2RR is a very complex reaction involving multiple proton and electron transfers. High sensitivity in situ electrochemical vibrational spectroscopy is a powerful tool to tackle this challenge.[17] Yeo and co-workers employed in-situ Raman spectroscopy revealing that the C2 products generation started after the reduction of surface CuO_x into metallic

Cu.[18] Koper et al. carried out a complementary IRAS and SERS study to clarify the role of supporting electrolyte and water content in determining products distribution for CO_2RR in an organic solvent.[19] By using attenuated total reflection surface enhanced infrared spectroscopy (ATR-SEIRAS), Xu et al. identified a CO adsorption band at 2058 cm^{-1} on oxide-derived Cu different from that on Cu-poly, and assigned it to the CO bound to the Cu(100) facet, which is responsible for its enhanced C2+ selectivity.[20] Waegele et al. used the same technique and clarified that atop-bound CO rather than bridge-bonded CO is an on-pathway intermediate for C1 and C2+ products.[21] It is thus of particular interest to extend *in situ* spectroscopic study of CO_2 reduction from monometallic Cu to metalloid-doped Cu electrodes.

In the present work, Cu film electrodes with or without metalloid B- (Cu-B) and P-doping (Cu-P) are fabricated by (electro) chemical plating method. By this means, we are able to comparatively study the distributions of the CO_2 reduction products over four different polycrystalline copper electrodes, i.e., mechanically polished Cu, electroplated Cu, chemically plated B-doped Cu and electroplated P-doped Cu. Both the plated Cu-B and Cu-P electrodes exhibit a significantly higher portion of C2+ products as compared to the un-doped counterparts in 0.1 M $KHCO_3$ electrolyte. Furthermore, *in situ* ATR-SEIRAS is extended to probe the potential dependent variation of the CO intermediates at the plated Cu, Cu-B and Cu-P film electrodes, to provide a correlation of the enhanced C2+ selectivity with the CO coverage.

Experimental

Preparation of plated Cu electrodes

The Cu foil (99.95%, 20 mm × 20 mm × 0.2 mm, Beijing Research Institute of Nonferrous Metals) was first mechanically polished with 1500-grit abrasive paper (STARCKE) to remove surface oxides. The freshly polished Cu foil was ultra-sonicated sequentially and repeatedly in acetone and Milli-Q water (> 18.2 MΩ·cm, Millipore), and eventually dried by a high purity nitrogen stream.

The polished Cu foil with its backside being sealed served as the substrate for electroplating or chemical plating a desired Cu film. Specifically, the un-doped Cu film was prepared by electrochemical deposition at -1.1 V (vs Ag/AgCl) for 100 s in a stirred aqueous solution consisting of 12 mM $CuSO_4$ and 0.11 M H_2SO_4 at room temperature; The electrodeposition of the Cu-P film was carried out in a stirred aqueous solution of 12

mM $CuSO_4 \cdot 5H_2O$, 0.48 M $NaH_2PO_2 \cdot H_2O$ and 0.034 M $Na_3C_6H_5O_7 \cdot 2H_2O$ at -1.1 V (vs Ag/AgCl) for 20 min at 70°C, with the plating bath pH adjusted to ca. 8 using a NH_4OH solution. The Cu-B film was chemically deposited according to the following procedures: 60 ml of a 12 mM $CuSO_4 \cdot 5H_2O$ + 0.034 M $Na_3C_6H_5O_7 \cdot 2H_2O$ solution was prepared, and its pH was adjusted to ca. 10.5 and its temperature was controlled at 55 °C; 2 mL of 0.1 g mL^{-1} DMAB solution prepared with cold water was injected quickly into the above $CuSO_4$ precursor solution under stirring, followed by placement of the polished Cu foil for 5 min.

The as-plated films were rinsed with copious amount of Milli-Q water and dried by the nitrogen stream for subsequent measurements.

Material characterizations

The surface morphologies of the plated films on Cu foil were characterized by a scanning electronic microscopy (SEM, FEI, Quanta 450 FEG). The crystalline phases of the plated films were characterized by a powder X-ray diffractometer using Cu Kα radiation from 35º to 80º (Bruker D2 Phaser). The surface electronic structures of the plated films were analyzed by using an ESCALAB 250 XI X-ray photoelectron spectrometer (Thermo Scientific) with the monochromatic Al Kα radiation (1486.6 eV), and the binding energies were calibrated with reference to the C 1s peak at 284.6 eV. To quantify the chemical compositions of the plated Cu-B and Cu-P electrodes, these two films were firstly deposited onto carbon paper substrates following the same protocol above, then dissolved into freshly prepared aqua regia. Inductively coupled plasma-atomic emission spectroscopy (ICP-AES, Thermo Elemental IRIS Intrepid) was employed to analyze the compositional information. *Ex situ* X-ray absorption spectrometry on the Cu K-edge was performed at the BL14LW beamline, Shanghai Synchrotron Radiation Facility, by recording the fluorescence signals of electroplated Cu, Cu-B and Cu-P on carbon paper, respectively.

CO_2RR Electrochemical measurements

All CO_2 reduction measurements were run at room temperature in a customized H-type two compartment glass cell separated by a Nafion 117 membrane with gas inlets and outlets. Each compartment contained 50 mL of 0.1 M $KHCO_3$ electrolyte. The solution in the cathodic compartment was purged with CO_2 (Air liquide, 99.999%) for 40 min prior to the start of electrolysis. A constant flow rate of CO_2 gas (30 sscm, monitored by Alicat Scientific mass flow controllers) was continuously delivered into the cathodic compartment to keep CO_2-saturation during electrolysis. A plated Cu film served the working electrode with a bunch of graphite rods and

a Ag/AgCl electrode used as the counter electrode and reference electrode, respectively. A CHI 660b electrochemical workstation was employed for the potential control and current measurement. All potentials reported were converted to the reversible hydrogen electrode (RHE) scale in this work using $E\ (\mathrm{vs.\,RHE}) = E\ (\mathrm{vs.\,Ag/AgCl}) + 0.199\ \mathrm{V} + 0.0591 \times \mathrm{pH}$ (herein pH 6.8), with a manual iR drop compensation (70% of the determined value). Before the start of a CO_2RR measurement, the electrode was subjected to the potential cycling from -0.54 V to 1.16 V vs RHE in an Ar-saturated 0.1 M $KHCO_3$. The electrochemical active surface area (ECSA) of a plated sample was estimated via its double layer capacitance by measuring and plotting the double layer charging current as a function of scan rate.

Quantification of CO_2RR products

The gas products were analyzed by an online gas chromatography (GC) with a Gas Chromatograph 2060 from Shanghai Ramiin Instruments equipped with a flame ionization detector (FID) coupled with a methanizer and a thermal conductivity detector (TCD). The detection limits of CO on FID, and H_2 on TCD, are determined to be 1 and 5 ppm, respectively. The FID was used to quantify hydrocarbons, CO, CO_2 and the TCD to quantify H_2. The gas products were sampled after a continuous electrolysis of ~15 min under each potential. The aqueous products were analyzed by a 500 MHz nuclear magnetic resonance (NMR) spectrometer from Bruker Company with a water suppression technique. Typically, 700 μL of the electrolyte after 2 h's electrolysis was mixed with 35 μL of D_2O solution containing phenol as the internal standard.

In-situ ATR-SEIRAS measurements

The Cu-B, Cu-P or Cu overfilm plated on a Au-coated reflecting plane of semicylindrical Si prism was used as the working electrode for in situ ATR-IR measurement, with the Ag/AgCl electrode and the graphite rod as the reference and counter electrodes, respectively. The infrared spectra were acquired by using a Thermoelectric IR spectrometer (Thermo Fisher IS50) equipped with an MCT-A detector at a spectral resolution of 8 cm^{-1} and with an unpolarized IR radiation at an incidence angle of ca. 65º. All the spectra are shown in the absorbance unit as -log (I/I_0), where I and I_0 represent the intensity of the reflected radiation of the sample and reference spectra, respectively. Experimental details including chemical deposition of the Au films, setup of ATR cell etc., can be found elsewhere.[22]

Results and Discussion

DMAB, as a reducing reagent and a boron source, initially used for wet chemical synthesis of Pd-B/C catalyst by our group,[13, 23] is further extended in this work for chemically plating the Cu-B film on a polished Cu substrate under modified reaction conditions. One-step electroplating of the Cu-P film was also tested here using $Na_2H_2PO_2$ as the phosphorus source. Typical SEM images of the mechanically polished Cu foil, electroplated Cu, chemically plated Cu-B and electroplated Cu-P films are shown in **Figure 1(a-d)**, respectively. In comparison to the bare substrate with relatively flat surface, the Cu-B film largely consists of densely packed nanoparticles, the Cu-P film consists of nanoflakes whereas the electroplated Cu film appears to have a densely packed underlayer scattered with larger nanoparticles on its top.

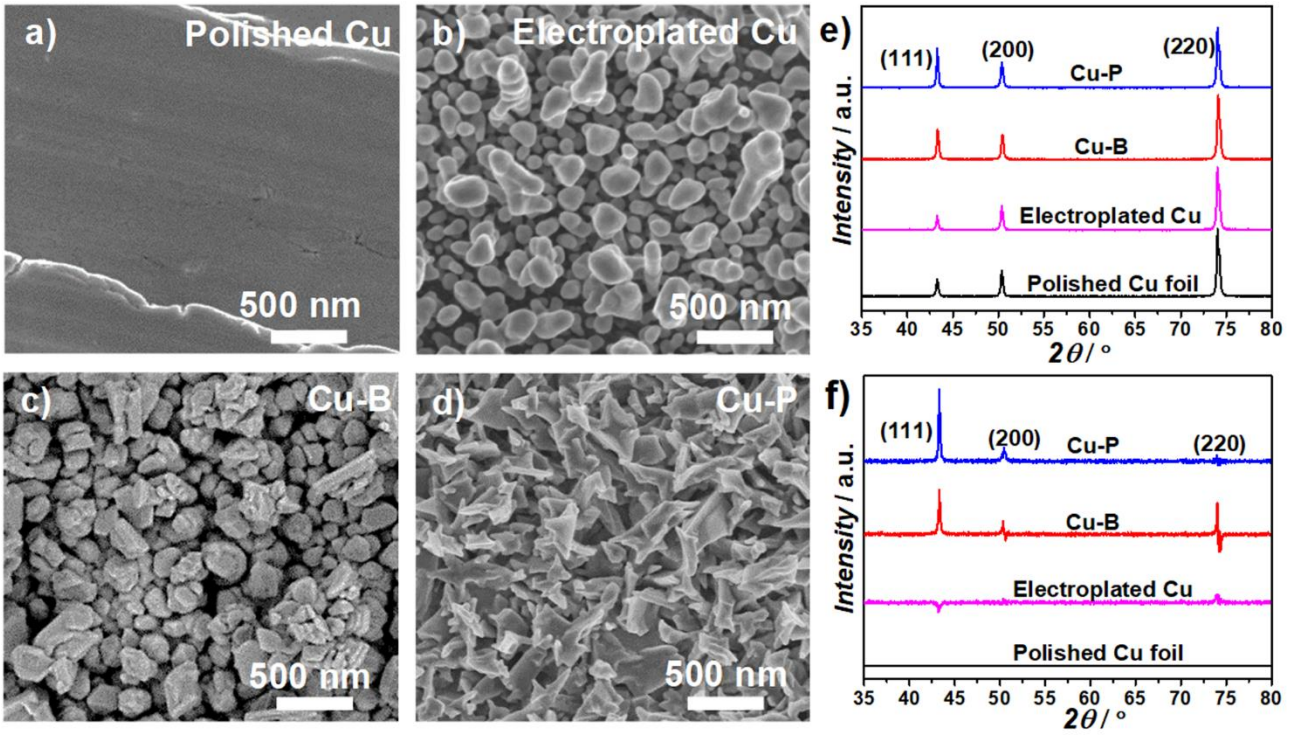

Figure 1. SEM images of the plated (a) polished Cu, (b) electroplated Cu, (c) Cu-B and (d) Cu-P. (e) symmetric XRD patterns of mechanically polished Cu (black), electroplated Cu (purple), Cu-B (red) and Cu-P(blue) electrodes. (f) Further XRD pattern subtraction is performed by employing the polished copper foil as the reference sample with the (220) peak intensity of each sample being normalized.

The symmetric XRD characterizations suggest polycrystalline features for these four Cu electrodes (**Figure 1e**), without any detectable copper oxide phases, although the Cu foil substrate has the (220) preferred texture. The diffraction peaks at 2θ degrees of 43.46º, 50.62º and 74.40º are indexed to the crystal planes of Cu(111), (200) and (220), respectively (JCPDS 04-0836). Since all the Cu electrodes show a predominant texture of Cu(220) from the underlying Cu foil, a simple subtraction is performed by normalizing the Cu(220) peak

intensity and then using the polished Cu foil as the reference to emphasize the crystalline structure of the plated Cu films (**Figure 1f**). After subtraction, the diffraction peaks are very weak for the electroplated Cu film, indicating approximately similar crystalline phases of the plated Cu film on the Cu foil. On the contrary, prominent (111) and relative weak (200) peaks are observed on the plated Cu-B and Cu-P films, suggesting the polycrystalline feature with certain (111) preference. Also, noted are the typical bipolar features at 74.4 º and 50.6 º in **Figure 1f** with the upward lope at a smaller angle and the downward lope at a larger angle due to a slightly negative shift of diffraction angles for the Cu-B film, suggesting an effective B doping in the Cu nanoparticle subsurface. In comparison, the XRD characteristic angles for the electroplated Cu-P film appear less shifted, suggestive of a significantly lower doping concentration of P or a different form of doping. The presence of B (or P) in the resulting Cu-B or (Cu-P) film can be further demonstrated by the XPS measurement (*vide infra*). Furthermore, a similar grain size distribution for the above electrodes is revealed upon calculating their (111) diffraction peaks by Scherer equation, i.e., 28.0, 30.8, 28.2 and 32.0 nm for polished Cu, plated Cu, Cu-B and Cu-P, respectively.

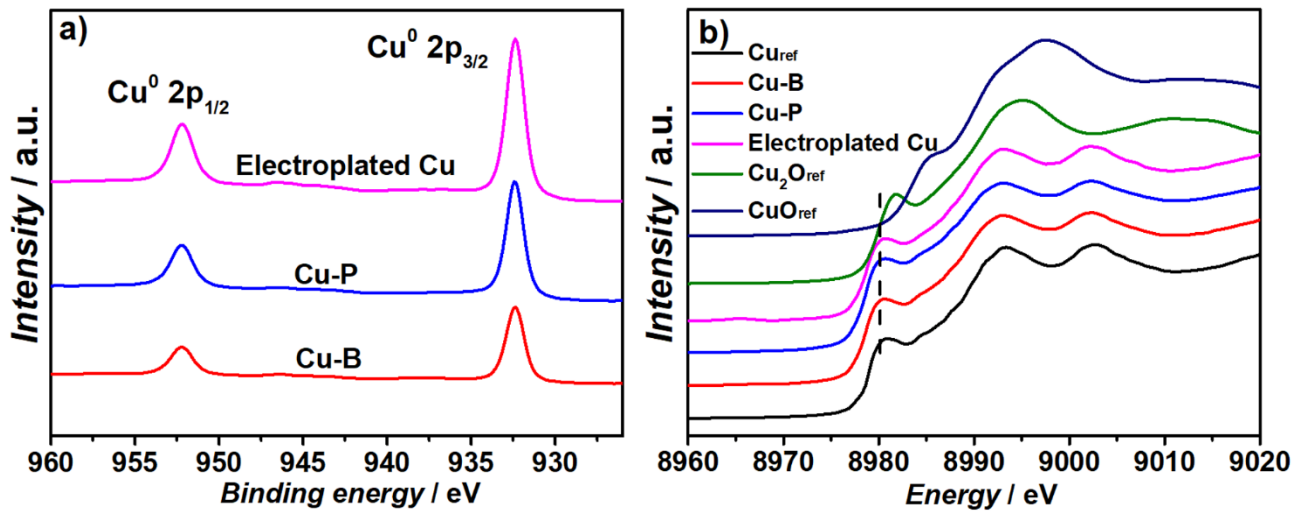

Figure 2. (a) X-ray photoelectron spectroscopy and (b) Cu K-edge X-ray absorption spectra of electroplated Cu, Cu-B, Cu-P electrodes, together with other reference samples.

The chemical states of Cu surface layers in the plated Cu, Cu-B and Cu-P films are first studied by *ex situ* core-level X-ray photoelectron spectroscopy (XPS). As shown in **Figure 2a**, two sharp peaks centered at ca. 932.4 eV and 952.2 eV in the Cu 2p region are observed for the Cu-B, Cu-P and Cu films, which can be attributed to Cu^0 $2p_{3/2}$ and Cu^0 $2p_{1/2}$, respectively.[7a] This metallic Cu feature can also be seen from the Cu Auger spectra (**Figure S1**),[24] and further reinforced by synchrotron radiation Cu K-edge X-ray absorption near-edge spectra (XANES, **Figure 2b**). In contrast to the Cu(I)/(II) oxide feature on Cu_2O and CuO references, a same

absorption edge at 8979 eV are observed corresponding to Cu(0) for all 3 plated samples and in accordance with standard Cu foil reference. No metal impurities are detected based upon the XPS survey spectra (**Figure S2**) and no relevant metalloid doping is found in the electroplated Cu film (**Figure S3**), while both the B 1s signal for the Cu-B film and the P 2p signal for the Cu-P film (as shown in the core level XPS spectra in **Figure S4** and the ICP-AES spectra in **Figure S5**) are clearly observed. These suggest that DMAB and NaH_2PO_2 serve as the effective B and P sources, respectively. It is noted that though some oxygen and carbon signals are observed on the XPS survey spectra, Cu 2p XPS, K-edge XANES, together with XRD and Auger analysis all suggest a metallic surface state for the above plated Cu electrodes. Therefore, we prudently assign these O and C signals to the surface adsorbed CO_2 and O_2 species due to the sample exposure to air during the transfer process.

10.1002/cctc.201901748

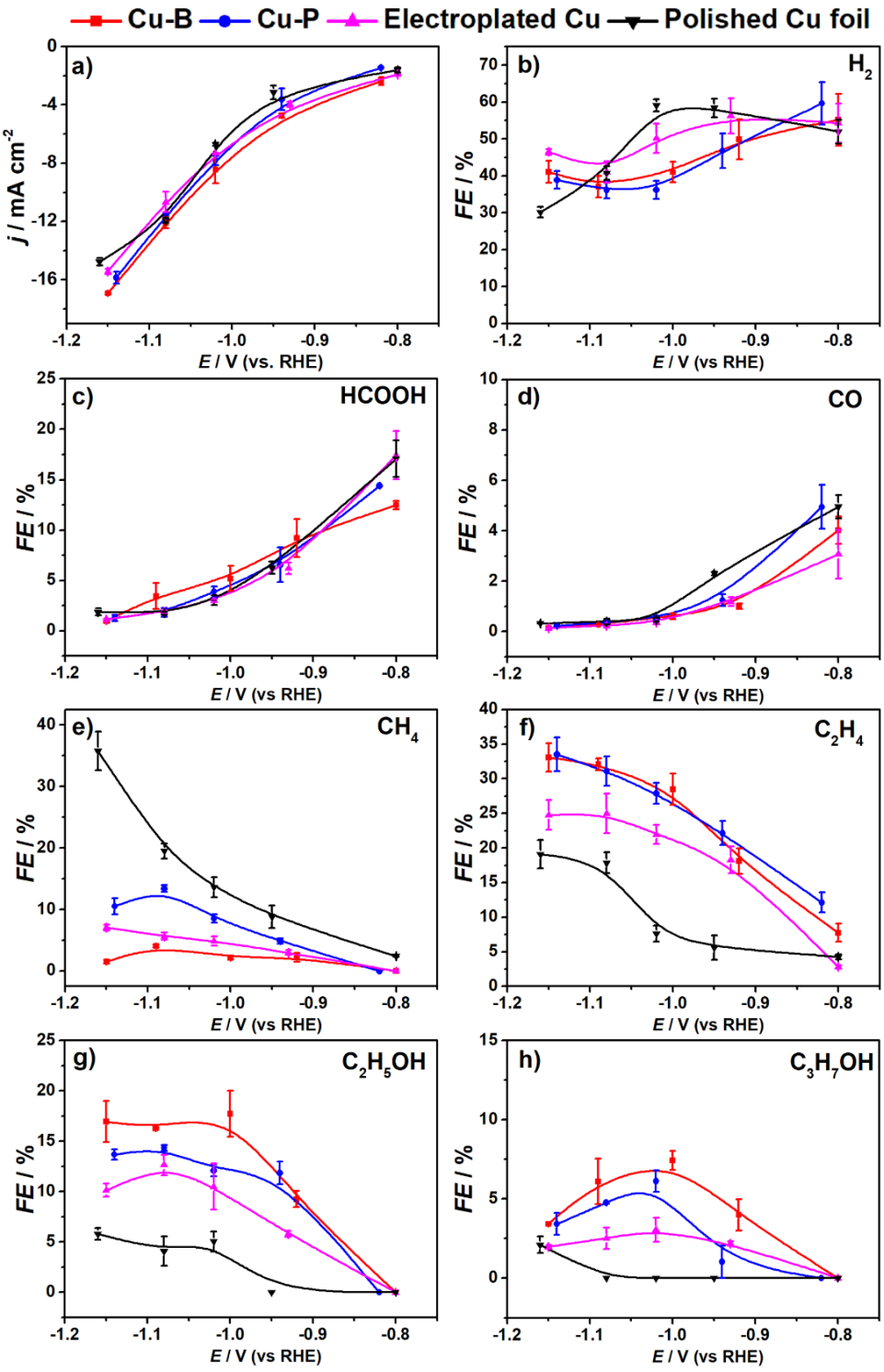

Figure 3. (a) Steady-state current densities averaged from 2-h CO_2RR electrolysis at each applied potential, together with the Faradaic efficiencies of (b) H_2, (c) $HCOO^-$, (d) CO, (e) CH_4, (f) C_2H_4, (g) ethanol (C_2H_5OH), and (h) n-propanol (C_3H_7OH) for Cu-B, Cu-P, electroplated Cu and polished Cu foil electrodes. The error bars represent two independent samples.

Chronoamperometric CO_2 reduction was performed over four different Cu electrodes at fixed potentials between -0.8 and -1.15 V in CO_2-saturated 0.1 M $KHCO_3$ electrolyte (pH 6.8). The gas products were analyzed

by gas chromatography (**Figure S6**), and the liquid products by nuclear magnetic resonance spectroscopy (**Figure S7**). The averaged geometric current densities at each applied potential were plotted in order to evaluate the electrocatalytic activities of the plated Cu- B, Cu-P, Cu films and the polished Cu foil, as shown in **Figure 3a** while the linear sweep voltammetry curves are plotted in **Figure S8**. Electrochemical surface areas of the four Cu electrodes are evaluated based upon their double layer capacitance measurements (**Figure S9**). Throughout the interested potential window, all the four Cu electrodes deliver a similar overall current density but a very different product selectivity. FEs for H_2 and other CO_2 reduction products as a function of applied potential are plotted in **Figure 3b-h**, for which the sum up efficiencies for all major products are ca. 82-105% (**Figure S10**). As compared to the polished Cu and the plated Cu, both Cu-B and Cu-P films show a lower selectivity toward H_2 evolution side reaction. FEs for formate and CO keep decreasing with negatively going potential on all Cu electrodes, while FE for CH_4 keeps increasing especially for the mechanically polished Cu. The maximum overall FE for C2+, i.e., 54.5% is recorded at ~ -1.08 V vs. RHE on the Cu-B electrode, consisting of 32.1% for C_2H_4, 16.3% ethanol and 6.1% n-propanol. Similarly, the Cu-P electrode also demonstrates an enhanced C2+ FE as compared to the un-doped Cu, reaching up to 50.3% at ~ -1.15 V (vs. 37.8% on the electroplated Cu and 26.9% on the polished Cu, **Figure S11**) including 33.5% for C_2H_4, 13.7% ethanol and 3.4% n-propanol.

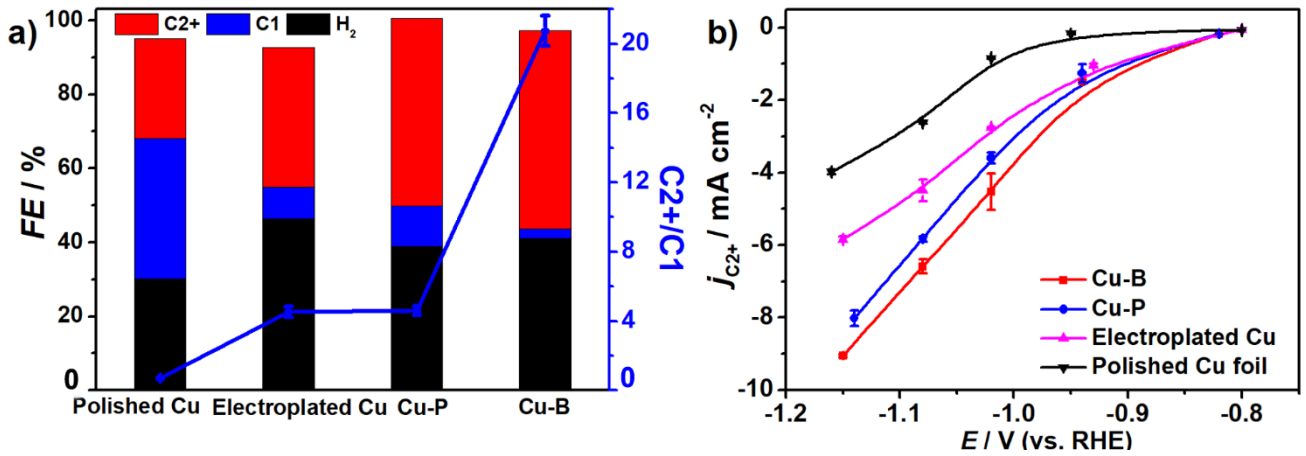

Figure 4. (a) Faradaic efficiencies for different Cu electrodes at ~ -1.15 V (vs RHE). (b) Partial current densities of C2+ products for different Cu electrodes as a function of potential.

To better compare the C2+/C1 selectivity on different Cu electrodes investigated, the distribution histograms of CO_2RR products at ~ -1.15 V with maximum C2+ FEs are plotted, together with the scatter plot showing the

corresponding C2+/C1 values in **Figure 4a**. The overall CO_2RR FEs (apart from H_2 evolution) are ca. 64.9% for the polished Cu, 46.1% for the electroplated Cu, 56.1% for the chemically plated Cu-B and 62.6% for the electroplated Cu-P, respectively. The highest current faradaic efficiency ratio of C2+/C1 is achieved on the Cu-B electrode (ca. 20.3) with an overall C2+ FE of 53.5%, which presents a 4.5-fold enhancement as compared to the electroplated Cu film, or a 29.0-fold enhancement over the polished Cu foil. Similarly, for the Cu-P electrode, we achieved a C2+/C1 ratio of 4.6, which is about a 6.5-fold improvement over the polished Cu. The overall C2+ partial current densities are also plotted in **Figure 4b**, both the Cu-B and Cu-P electrodes surpass the un-doped Cu ones for selective generation of the C2+ products over the whole potential window. Specifically, at ~ -1.15 V vs RHE, the Cu-B film delivers 9.0 mA cm^{-2}, and the Cu-P film 8.0 mA cm^{-2} for the C2+ partial current density, which is 2.3-fold and 2.0-fold as high as the polished Cu, respectively. Besides, throughout the interested potential window from -0.80 V to -1.15 V vs RHE, the multi-carbon product generation activities (partial current densities) on the Cu-B and Cu-P films surpass those on the polished Cu foil by a factor up to 5.4 and 4.3 at ~ -1.0 V vs RHE, respectively.

Since a similar geometric current density is observed for all the Cu electrodes (**Figure 3a**), the local pH change due to proton consumption at cathode surface is unlikely the major contributor to this observed selectivity change. Furthermore, the traditional viewpoint on the crystalline plane effect is that the (111) facet is not favorable for C2+ product selectivity. In the meanwhile, SEM characterizations suggest these four polycrystalline Cu electrodes show quite different morphologies of secondary particle packing density and grain boundary density, which could potentially contribute to altering the CO_2RR product distribution. To better address this morphology effect, we have prepared another Cu-B film electrode with a prolonged chemical plating time of 12 min. As shown in **Figure S12**, the 5-min and 12-min Cu-B samples show a different morphology but a similar subsurface B doping content from DMAB, as a matter of fact, both of them demonstrate an enhanced C_2H_4/CH_4 selectivity as compared to the electroplated Cu, thus highlighting the metalloid doping effect as a main factor for promoting the C-C bond formation in this study. In fact, according to the DFT calculations,[15a] the B- doped Cu (111) electrode can greatly improve the C2+ products selectivity as compared to the B-doped Cu (100) electrode by decreasing the energy barrier for the C-C coupling during the CO_2RR, in agreement with our experimental data.

To track the real-time surface intermediate information during the CO_2RR over these plated Cu electrodes, high sensitivity in situ electrochemical ATR-SEIRAS measurements are performed on Cu-B, Cu-P, and

electroplated Cu film electrodes on Au-coated Si prism.[22] **Figure 5a to 5c** show the ATR-SEIRAS spectra acquired during negative-going potential sweep in CO_2-saturated 0.1 M $KHCO_3$. For all the three Cu film electrodes, linearly bonded CO (CO_L) from CO_2 reduction shows up at ~ -0.38 V vs. RHE and thereafter, at frequencies of ~ 2060-2077 cm^{-1}.[25] The adsorbed CO bands are gradually blue-shifted with increasing band intensities due to the dipole-dipole coupling effect as the potential moves stepwise from ~ -0.4 to ~ -0.7 V, and then red-shifted at more negative potentials (< ~ -0.7 V, toward a more negatively charged surface) due to the Stark effect, which is consistent with previous reports.[25a, 26]

We further integrate the CO_L band intensities as a function of applied potential for these plated Cu electrodes, as depicted in **Figure 5d**. In the negative going potential sweep, the maximum CO_L band intensity locates at -0.67 V for Cu-B (red), -0.71 V for Cu-P (blue) and -0.76 V for Cu (black), respectively. Moreover, with more negative potential applied, the $\nu(CO_L)$ band on Cu-B or Cu-P decreases more rapidly than that on electroplated Cu though at a similar overall current density. It is known that *CO on Cu surfaces can go through three different pathways: 1) get directly released from surface as CO(g), 2) via *CHO pathway to form CH_4(g), 3) via C-C coupling step to form C2 and C3 products.[27] Herein, by on-line GC quantification analysis of CO(g) and CH_4(g) products (**Figures 3d and 3e**), it is found that both pathway (1) and pathway (2) are suppressed with B- doping and pathway (1) is suppressed with P-doping. Given the superior C2+ generation performance on Cu-B and Cu-P (**Figure 3f-h**) as compared to those on electroplated Cu, this rapid consumption of *CO on Cu-B and Cu-P contributes mainly to the enhanced multi-carbon product generation from a more facile pathway (3) of C-C coupling step. Specifically, even faster consumption of *CO on Cu-P at potentials negative of -0.95 V may come from concurrent enhancement of pathway (2).

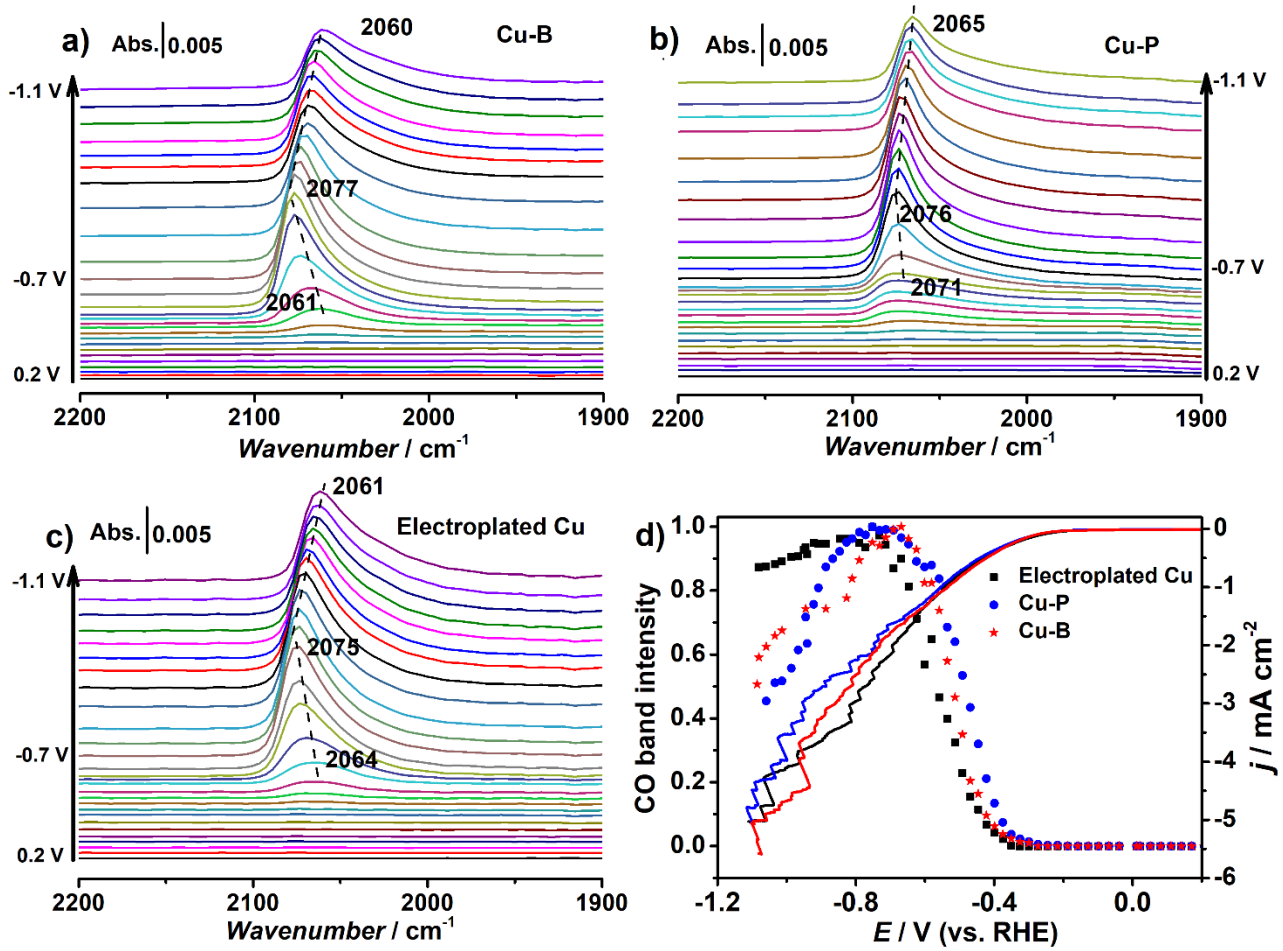

Figure 5. In situ electrochemical ATR-SEIRAS spectra of CO on (a) Cu-B, (b) Cu-P, and (c) electroplated Cu electrodes in CO_2-saturated 0.1 M $KHCO_3$ solution. (d) the integrated band intensity of linearly adsorbed CO (CO_L) on Cu-B, Cu-P and electroplated Cu electrodes as the function of cathodic potential, respectively and LSV curves obtained on Cu-B, Cu-P, and electroplated Cu electrode at a scan rate of 1 mV s^{-1} in CO_2-saturated 0.1 M $KHCO_3$ solution.

Conclusion

In summary, we have investigated the electrochemical CO_2 reduction on four kinds of plated polycrystalline Cu electrodes. Ex situ XPS, Auger and XANES analysis suggest a metallic Cu surface structure regardless the plating condition. With the metalloid doping, both Cu-B and Cu-P exhibit an enhanced selectivity toward multi-carbon products generation, At -1.15 V vs. RHE, 53.5% and 50.3% Faradaic efficiency (FE) toward C2+ products generation are observed on the Cu-B and Cu-P electrodes in 0.1 M $KHCO_3$, demonstrating a 29.0- and 6.5-times enhancement of C2+/C1 ratio as compared to the polished Cu electrode, respectively. Besides, throughout the interested potential window from -0.80 V to -1.15 V, the multi-carbon product generation activity (partial current density) on Cu-B and Cu-P surpass the polished Cu foil by a factor up to 5.4 times and 4.3 times

at ~ -1.0 V vs RHE, respectively. Comparative study on these plated Cu film electrodes by in situ electrochemical ATR-SEIRAS reveals a more facile conversion of linear bounded *CO intermediate on Cu-B and Cu-P surfaces as compared to un-doped Cu. Furthermore, in considering together on-line GC/NMR products quantification and *in situ* ATR-SEIRAS analysis, we find that P-doping leads to a concurrent enhancement for both CH_4 and C2+ generation while B-doping leads to a significantly higher C2+/C1 selectivity as compared to electroplated Cu without metalloid doping, both are at the sacrifice of *CO surface intermediate.

Acknowledgements

This work was supported by the NSFC (Grant No. 21733004), the 973 Program of MOST (Grant No. 2015CB932303), and the International Cooperation Program of STCSM (Grant No. 17520711200). K.J. acknowledges the startup funding from Shanghai Jiao Tong University. We thank Mr. Kang Liu at Central South University for the assistance in XANES data analysis.

Keywords

Carbon dioxide reduction; Copper plating; Copper electrode; Metalloid doping; ATR-SEIRAS

References

[1] a) O. S. Bushuyev, P. De Luna, C. T. Dinh, L. Tao, G. Saur, J. van de Lagemaat, S. O. Kelley, E. H. Sargent, *Joule* **2018**, *2*, 825-832; b) P. Sebastián-Pascual, S. Mezzavilla, I. E. L. Stephens, M. Escudero-Escribano, *ChemCatChem* **2019**, *11*, 1-21.

[2] A. E. Farrell, R. J. Plevin, B. T. Turner, A. D. Jones, M. O'Hare, D. M. Kammen, *Science* **2006**, *311*, 506-508.

[3] a) A. A. Peterson, F. Abild-Pedersen, F. Studt, J. Rossmeisl, J. K. Norskov, *Energy Environ. Sci.* **2010**, *3*, 1311-1315; b) K. P. Kuhl, E. R. Cave, D. N. Abram, T. F. Jaramillo, *Energy Environ. Sci.* **2012**, *5*, 7050-7059; c) J. Fu, W. Zhu, Y. Chen, Z. Yin, Y. Li, J. Liu, H. Zhang, J. J. Zhu, S. Sun, *Angew. Chem. Int. Ed.* **2019**, *58*, 1-5.

[4] Z. Yin, G. T. R. Palmore, S. Sun, *Trends Chem.* **2019**, DOI: 10.1016/j.trechm.2019.05.004.

[5] a) Y. Hori, I. Takahashi, O. Koga, N. Hoshi, *J. Phys. Chem. B* **2002**, *106*, 15-17; b) F. Calle-Vallejo, M. T. Koper, *Angew. Chem. Int. Ed.* **2013**, *52*, 7282-7285; c) K. Jiang, R. B. Sandberg, A. J. Akey, X. Liu, D. C. Bell, J. K. Nørskov, K. Chan, H. Wang, *Nat. Catal.* **2018**, *1*, 111-119.

[6] a) T. T. H. Hoang, S. Ma, J. I. Gold, P. J. A. Kenis, A. A. Gewirth, *ACS Catal.* **2017**, *7*, 3313-3321; b) K. D. Yang, W. R. Ko, J. H. Lee, S. J. Kim, H. Lee, M. H. Lee, K. T. Nam, *Angew. Chem. Int. Ed.* **2017**,

56, 796-800; c) D. Raciti, K. J. Livi, C. Wang, *Nano Lett.* **2015**, *15*, 6829-6835; d) H. Wang, E. Matios, C. Wang, J. Luo, X. Lu, X. Hu, W. Li, *Nano Lett.* **2019**, *19*, 3925-3932.

[7] a) Y. X. Duan, F. L. Meng, K. H. Liu, S. S. Yi, S. J. Li, J. M. Yan, Q. Jiang, *Adv. Mater.* **2018**, *30*, e1706194; b) R. Reske, H. Mistry, F. Behafarid, B. Roldan Cuenya, P. Strasser, *J. Am. Chem. Soc.* **2014**, *136*, 6978-6986.

[8] a) P. De Luna, R. Quintero-Bermudez, C.-T. Dinh, M. B. Ross, O. S. Bushuyev, P. Todorović, T. Regier, S. O. Kelley, P. Yang, E. H. Sargent, *Nat. Catal.* **2018**, *1*, 103-110; b) M. G. Kibria, C. T. Dinh, A. Seifitokaldani, P. De Luna, T. Burdyny, R. Quintero-Bermudez, M. B. Ross, O. S. Bushuyev, F. P. Garcia de Arquer, P. Yang, D. Sinton, E. H. Sargent, *Adv. Mater.* **2018**, *30*, e1804867.

[9] a) X. Feng, K. Jiang, S. Fan, M. W. Kanan, *J. Am. Chem. Soc.* **2015**, *137*, 4606-4609; b) S. Lee, G. Park, J. Lee, *ACS Catal.* **2017**, *7*, 8594-8604; c) X. Feng, K. Jiang, S. Fan, M. W. Kanan, *ACS Cent. Sci.* **2016**, *2*, 169-174; d) A. Verdaguer-Casadevall, C. W. Li, T. P. Johansson, S. B. Scott, J. T. McKeown, M. Kumar, I. E. Stephens, M. W. Kanan, I. Chorkendorff, *J. Am. Chem. Soc.* **2015**, *137*, 9808-9811.

[10] S. Ma, M. Sadakiyo, M. Heima, R. Luo, R. T. Haasch, J. I. Gold, M. Yamauchi, P. J. Kenis, *J. Am. Chem. Soc.* **2017**, *139*, 47-50.

[11] a) T. T. H. Hoang, S. Verma, S. Ma, T. T. Fister, J. Timoshenko, A. I. Frenkel, P. J. A. Kenis, A. A. Gewirth, *J. Am. Chem. Soc.* **2018**, *140*, 5791-5797; b) Y. C. Li, Z. Wang, T. Yuan, D. H. Nam, M. Luo, J. Wicks, B. Chen, J. Li, F. Li, F. P. G. de Arquer, Y. Wang, C. T. Dinh, O. Voznyy, D. Sinton, E. H. Sargent, *J. Am. Chem. Soc.* **2019**, *141*, 8584-8591; c) J. Wang, Z. Li, C. Dong, Y. Feng, J. Yang, H. Liu, X. Du, *ACS Appl. Mater. Interfaces* **2019**, *11*, 2763-2767.

[12] Y. Feng, Z. Li, H. Liu, C. Dong, J. Wang, S. A. Kulinich, X. Du, *Langmuir* **2018**, *34*, 13544-13549.

[13] B. Jiang, X. G. Zhang, K. Jiang, D. Y. Wu, W. B. Cai, *J. Am. Chem. Soc.* **2018**, *140*, 2880-2889.

[14] a) Y. Deng, Y. Huang, D. Ren, A. D. Handoko, Z. W. Seh, P. Hirunsit, B. S. Yeo, *ACS Appl. Mater. Interfaces* **2018**, *10*, 28572-28581; b) K. R. Phillips, Y. Katayama, J. Hwang, Y. Shao-Horn, *J. Phys. Chem. Lett.* **2018**, *9*, 4407-4412; c) Z. Zhao, X. Peng, X. Liu, X. Sun, J. Shi, L. Han, G. Li, J. Luo, *J. Mater. Chem. A* **2017**, *5*, 20239-20243; d) T. Shinagawa, G. O. Larrazábal, A. J. Martín, F. Krumeich, J. Pérez-Ramírez, *ACS Catal.* **2018**, *8*, 837-844.

[15] a) Y. Zhou, F. Che, M. Liu, C. Zou, Z. Liang, P. De Luna, H. Yuan, J. Li, Z. Wang, H. Xie, H. Li, P. Chen, E. Bladt, R. Quintero-Bermudez, T. K. Sham, S. Bals, J. Hofkens, D. Sinton, G. Chen, E. H. Sargent, *Nat. Chem.* **2018**, *10*, 974-980; b) C. Chen, X. Sun, L. Lu, D. Yang, J. Ma, Q. Zhu, Q. Qian, B. Han, *Green Chem.* **2018**, *20*, 4579-4583.

[16] Z. Q. Liang, T. T. Zhuang, A. Seifitokaldani, J. Li, C. W. Huang, C. S. Tan, Y. Li, P. De Luna, C. T. Dinh, Y. Hu, Q. Xiao, P. L. Hsieh, Y. Wang, F. Li, R. Quintero-Bermudez, Y. Zhou, P. Chen, Y. Pang, S. C. Lo, L. J. Chen, H. Tan, Z. Xu, S. Zhao, D. Sinton, E. H. Sargent, *Nat. Commun.* **2018**, *9*, 3828.

[17] a) N. Heidary, K. H. Ly, N. Kornienko, *Nano Lett.* **2019**, *19*, 4817-4826; b) S. Zhu, T. Li, W.-B. Cai, M. Shao, *ACS Energy Lett.* **2019**, *4*, 682-689; c) S. Zhu, B. Jiang, W. B. Cai, M. Shao, *J. Am. Chem. Soc.* **2017**, *139*, 15664-15667; d) K. Yang, R. Kas, W. A. Smith, *J. Am. Chem. Soc.* **2019**, *141*, 15891-15900; e) R. Kas, O. Ayemoba, N. J. Firet, J. Middelkoop, W. A. Smith, A. Cuesta, *ChemPhysChem* **2019**, DOI: 10.1002/cphc.201900533.

[18] a) L. Mandal, K. R. Yang, M. R. Motapothula, D. Ren, P. Lobaccaro, A. Patra, M. Sherburne, V. S. Batista, B. S. Yeo, J. W. Ager, J. Martin, T. Venkatesan, *ACS Appl. Mater. Interfaces* **2018**, *10*, 8574-8584; b) D. Ren, J. Fong, B. S. Yeo, *Nat. Commun.* **2018**, *9*, 925.

[19] M. C. Figueiredo, I. Ledezma-Yanez, M. T. M. Koper, *ACS Catal.* **2016**, *6*, 2382-2392.

[20] A. S. Malkani, M. Dunwell, B. Xu, *ACS Catal.* **2018**, *9*, 474-478.
[21] C. M. Gunathunge, V. J. Ovalle, Y. Li, M. J. Janik, M. M. Waegele, *ACS Catal.* **2018**, *8*, 7507-7516.
[22] K. Jiang, H. Wang, W. B. Cai, H. Wang, *ACS Nano* **2017**, *11*, 6451-6458.
[23] J. Y. Wang, Y. Y. Kang, H. Yang, W. B. Cai, *J. Phys. Chem. C* **2009**, *113*, 8366-8372.
[24] a) F. Scholten, I. Sinev, M. Bernal, B. Roldan Cuenya, *ACS Catal.* **2019**, *9*, 5496-5502; b) M. B. Ross, C. T. Dinh, Y. Li, D. Kim, P. De Luna, E. H. Sargent, P. Yang, *J. Am. Chem. Soc.* **2017**, *139*, 9359-9363.
[25] a) C. M. Gunathunge, X. Li, J. Li, R. P. Hicks, V. J. Ovalle, M. M. Waegele, *J. Phys. Chem. C* **2017**, *121*, 12337-12344; b) J. Heyes, M. Dunwell, B. Xu, *J. Phys. Chem. C* **2016**, *120*, 17334-17341.
[26] a) S. Lee, J. Lee, *ChemElectroChem* **2018**, *5*, 558-564; b) G. Iijima, T. Inomata, H. Yamaguchi, M. Ito, H. Masuda, *ACS Catal.* **2019**, 6305-6319; c) A. Wuttig, C. Liu, Q. Peng, M. Yaguchi, C. H. Hendon, K. Motobayashi, S. Ye, M. Osawa, Y. Surendranath, *ACS Cent. Sci.* **2016**, *2*, 522-528.
[27] a) Y. Zheng, A. Vasileff, X. Zhou, Y. Jiao, M. Jaroniec, S. Z. Qiao, *J. Am. Chem. Soc.* **2019**, *141*, 7646-7659; b) A. J. Garza, A. T. Bell, M. Head-Gordon, *ACS Catal.* **2018**, *8*, 1490-1499; c) E. Perez-Gallent, M. C. Figueiredo, F. Calle-Vallejo, M. T. Koper, *Angew. Chem. Int. Ed.* **2017**, *56*, 3621-3624.

10.1002/cctc.201901748

Table of Contents Graphic

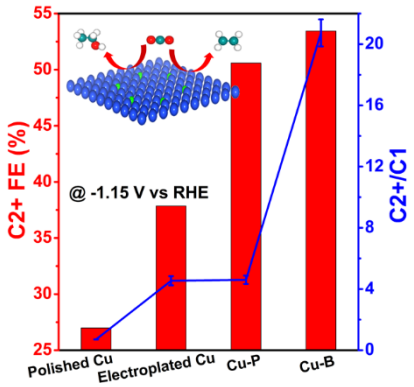

B- and P-doped Cu catalysts: metalloid-doping promotes C-C bond formation during electrochemical CO_2 reduction toward multi-carbon products on plated Cu-B and Cu-P film electrodes, in particular the Cu-B electrode yields a significantly higher C2+/C1 ratio.